Effects of lung inflation on alveolar epithelial solute and water transport properties

KWANG-JIN KIM AND EDWARD D. CRANDALL
Department of Medicine, University of California, Los Angeles, School of Medicine, Los Angeles, California 90024

KIM, KWANG-JIN, AND EDWARD D. CRANDALL. *Effects of lung inflation on alveolar epithelial solute and water transport properties.* J. Appl. Physiol.: Respirat. Environ. Exercise Physiol. 52(6): 1498–1505, 1982.—Paired hollow bullfrog lungs (*Rana catesbeiana*) were used to study the effects of lung inflation on alveolar epithelial transport of water and hydrophilic solutes. Frogs were double pithed and the lungs were removed after bronchial placement of a Lucite plug. Three openings in the plug accommodated the insertion of two agar-Ringer bridges (for electrical potential measurement and passage of direct current) and the injection and removal of alveolar bathing fluid. Ringer solution containing a tracer quantity of radioactive solute was instilled into the lung sacs (5 ml or 50 ml) and the lungs were suspended in baths of Ringer solution containing appropriate cold solutes (5 mM). Permeability properties of each solute (and water) were determined from the rate of radiotracer concentration change in the bath. The spontaneous potential difference, tissue resistance, and solute permeability properties determined in these experiments showed no significant differences between the 5- and 50-ml lungs. Assuming homogeneous, cylindrical water-filled pores to be present in the tissue, the equivalent pore radii estimated from the rates of solute and water fluxes were 1.1 (for 5-ml lungs) and 0.9 nm (for 50-ml lungs). After overinflation of the lung (to >80 ml), experiments at 50 ml yielded a pore radius of 3.4 nm. These data suggest that passive alveolar epithelial transport properties do not change with degrees of lung inflation normally encountered in vivo but that overinflation can lead to increased leakiness of the barrier.

epithelium; bullfrog; pore

BOTH MORPHOLOGICAL and physiological studies have shown that the pulmonary epithelial barrier, which helps separate the air space from the vascular space in the lung, plays the dominant role in preventing the leak of water and solutes from blood and interstitium into alveoli. Pietra et al. (19, 20) showed that intravascular tracer hemoglobin did not appear in the air space of the dog lung until 70 Torr pulmonary arterial pressure was reached, although it was found in the interstitial space at 50 Torr pulmonary arterial pressure. Schneeberger and Karnovsky (24, 25) presented morphological evidence in mouse lungs, using horseradish peroxidase as an ultrastructural tracer, that epithelium is a more effective barrier than endothelium in that tracer could be seen to cross the endothelial junctions readily but was stopped by the epithelial tight junctions. Similar observations were made using the smaller tracer, cytochrome *c* (22). Schneeberger (23), using freeze-fracture techniques, found that the alveolar epithelial cell junctions are joined by a much more complex network of strands than are endothelial cell junctions in mammalian lungs.

In physiological studies, Taylor and Gaar (27) used data from isolated dog lungs to calculate that the equivalent pore radius in the pulmonary epithelium is 0.6–1.0 nm, compared with that in the pulmonary endothelium of 7.5 nm. Taking advantage of the normally fluid-filled state of fetal lungs, Normand et al. (17) showed that the fetal lamb lung epithelium is very resistant to solute flow (pore radius of 0.55–0.61 nm for epithelium vs. 15 nm for endothelium). Theodore et al. (28) presented evidence that there may be a small population of larger (>8 nm radius) pores present in the pulmonary epithelial barrier. Wangensteen et al. (30) concluded, in their rabbit lung studies, that the resistance to lipid-insoluble solute transport across the blood gas barrier is due primarily to the alveolar epithelium. These physiological studies, and the morphological studies cited above, are consistent with the conclusion that pulmonary epithelium is the primary barrier to the flow of water and solutes from vascular space to alveoli.

Egan et al. (5) suggested that epithelial permeability in the sheep lung increases gradually with increases in lung inflation. They further suggested that there is a critical inflation pressure (about 35 cmH_2O) at which the pulmonary epithelium becomes very leaky to solutes. Egan et al. (5) postulated that as the lung epithelium is progressively stretched, water-filled channels between alveolar cells gradually widen. It was further suggested that at high inflating pressures and at inflation volumes that were close to total lung capacity, resistance to hydrophilic solute transport is lost entirely and the alveolar epithelium no longer functions as an effective barrier between the circulation and the air spaces. In recent studies of changes in solute permeability across lung epithelium at different consecutive lung volumes in the same lung of anesthetized dogs, Egan (4) found that the increased pore radius present at higher physiological lung volumes does not diminish when volume is reduced, suggesting the phenomenon represents lung injury affecting intercellular junctions at high (but physiological) lung inflation volumes.

Although the above results are interesting and useful, they are subject to serious theoretical and practical problems related to interpretation of data obtained in mammalian lung studies. Both the volumes of distribution of

0161-7567/82/0000-0000$01.25 Copyright © 1982 the American Physiological Society

Downloaded from http://jap.physiology.org/ by 10.220.33.3 on September 15, 2016

the test solutes and the surface area available for the transfer of water and solutes across the lung barrier are unknown. The series arrangement of the parts of the barrier (epithelium, interstitium, endothelium) complicates inferences about rate-limiting factors. There are at least two parallel (airway and alveolar) epithelial barriers that may have different solute and water permeability characteristics. Recent reports showed that the hydraulic conductance of tracheal epithelium, about 4×10^{-12} ml/dyn·s (32), is about an order of magnitude greater than that for alveolar epithelium. The latter problem is of particular importance, since a report has recently appeared suggesting that alveolar edema fluid may be formed by retrograde filling of alveoli with solutes and water that were directly transferred across airway epithelium (8). Finally, unstirred layers in fluid-filled mammalian lung studies are probably very large, virtually impossible to measure, and have never been taken into account in transport studies.

A recent important morphological observation also leads to some difficulty in understanding the results from mammalian lung epithelial permeability studies as a function of lung inflation. Gil et al. (9) have shown that mammalian lung inflation involves "depleating" of alveolar walls, rather than stretching. As a result, it is difficult to envision the mechanism for pore enlargement with inflation at physiological lung volumes.

To study alveolar epithelial transport properties more directly, the simple model of the hollow bullfrog lung mounted in the Ussing chamber has recently been utilized (1, 6, 7). Frog lung alveolar epithelium is a continuous layer of epithelial cells that have characteristics of both type I and type II cells of mammalian alveolar epithelium (18). It has been found that the bullfrog lung generates a spontaneous potential of about 20 mV, with a tissue resistance being about 2 kΩ·cm^2 (1). The passive solute and water permeability properties of this tissue are very similar to those of other "tight" epithelia (e.g., toad urinary bladder) with an equivalent homogeneous pore radius of about 0.8 nm.

In the studies reported here, we developed a sac preparation of the bullfrog lung to investigate its bioelectric and permeability properties at different lung volumes. Paired lungs from the same animal were utilized to study the effects of physiological lung inflation (5 ml and 50 ml). In one series of experiments, one lung of the pair was overinflated (to >80 ml) before being studied at 50 ml. Our results suggest that none of the properties studied (including pore radius) is a function of inflation volume in the physiological range, although the alveolar epithelium became somewhat leaky after overinflation.

MATERIALS AND METHODS

Tissue preparation. North American bullfrogs (*Rana catesbeiana*) were used in these experiments. After double pithing the animal the chest was opened, and the median portion of the pectoral girdle was removed. After incising the laryngeal covering of the glottis, a separate Lucite plug was inserted through the glottal opening into the bronchus of each lung. A thin film of silicone high-vacuum grease (Dow Corning, Midland, MI) had been applied to the outside of the plug to help minimize subsequent tissue damage. The Lucite plug was constructed with three openings to accommodate insertion of agar-Ringer bridges and a three-way stopcock (Fig. 1*A*). A suture was tied around the bronchial portion of the lung encircling the Lucite plug using cotton umbilical tape (10A, Ethicon, Somerville, NJ). Each lung was isolated by careful incision across the bronchus proximal to the suture. The inside of each lung sac was then filled with Ringer solution to a predetermined volume through the stopcock and mounted as a sac preparation in a 150- to 200-ml reservoir of amphibian Ringer solution (Fig. 1*B*). The surfaces of the internal and external Ringer solutions were at the same level at atmospheric pressure. Agar-Ringer bridges were inserted through the Lucite plug into the internal fluid and into the external reservoir for potential measurement and passage of direct current.

The amphibian Ringer solution used had the following composition (in mM): NaCl 110.0, $NaHCO_3$ 2.4, KCl 2.4, $CaCl_2$ 1.0, glucose 5.5. The pH of the solution after equilibration with room air was about 8.0. All experiments were performed at room temperature (22–25°C).

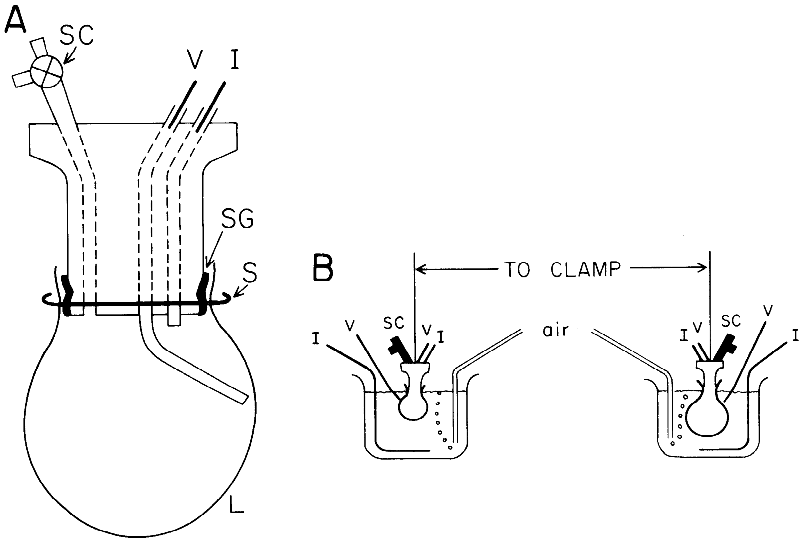

FIG. 1. Schematic diagram of paired bullfrog lungs mounted as sac preparations. Plug was inserted through glottal opening into bronchus of each lung. *A:* detail of lung. L, lung; V, port for potential measurement; I, port for current passage; S, suture; SC, three-way stopcock for insertion and removal of alveolar fluid; SG, silicone high-vacuum grease. *B:* experimental set-up of paired lungs.

Downloaded from http://jap.physiology.org/ by 10.220.33.3 on September 15, 2016

At the end of several experiments, the tissue was fixed with either 10% formalin or Zenker's solution, embedded in paraffin, sectioned, and stained with EVG (Verhoeff van Gieson) for light microscopy.

Experimental procedure. Lungs from the same animal were paired to investigate the effects of different inflation volumes on bioelectric properties and alveolar epithelial permeability to water and solutes. One lung was inflated to 5 ml and the other to 50 ml. These volumes were chosen as representative of low- and high-inflation volumes of bullfrog lungs in vivo. After filling but before suspending the lungs in the external reservoir of Ringer solution, the lung sac preparation was inspected carefully for leaks.

In one series of experiments, one lung was inflated to 50 ml and the other lung was purposely damaged by inflation to over 80 ml of lung volume. When the lung was inflated to above 80 ml, the Ringer solution inside the sac was observed to appear on the outer lung surface, which had been previously dry. After keeping the damaged lung above 80 ml for 15 min, the alveolar fluid was drained and fresh solution was instilled to a final inflation volume of 50 ml. This lung was paired with the undamaged lung inflated to 50 ml to study the effects of lung overinflation on alveolar epithelial bioelectric and permeability properties. Electrical potential difference, tissue resistance, and tracer fluxes of water and solutes across the alveolar epithelium were measured in each suspended lung.

Electrical measurements. The electrical potential difference across the tissue was measured using a matched pair of calomel half cells (Fisher Scientific, Philadelphia, PA) with connecting agar-Ringer bridges. Agar bridges were made of polyethylene tubing (PE-200, Fisher Scientific, Philadelphia, PA) with 4% agar in Ringer solution. The distance between the tips of the agar bridges and the tissue for the potential measurements was about 0.2 cm. Current was passed across the tissue via a pair of Ag/AgCl electrodes and connecting agar bridges. The distance between the bridges and the tissue was about 5 cm. When there was no current applied across the tissue, the measured potential difference (PD) was designated as spontaneous potential difference (SPD). Tissue resistance (R_t) was estimated from the relationship $\mathrm{d}V/\mathrm{d}I$, where $\mathrm{d}I$ is the amount of current instantaneously applied across the tissue and $\mathrm{d}V$ is the voltage change across the tissue in response to $\mathrm{d}I$. The instantaneous $\mathrm{d}I$ was obtained using a function generator (model 5700, Krohn-Hite, Avon, MA).

Permeability measurements. Diffusion of water, urea, ethylene glycol, arabinose, sucrose, and raffinose were studied in paired bullfrog lungs from the same animal using radioactive tracers. The direction of diffusion was always from the alveolar to the pleural surface. All the bathing fluids contained appropriate added cold solute(s) at a concentration of 5 mM. Five to fifty microcuries of radioisotopic material(s) (water, arabinose, and raffinose were labeled with ^{3}H, others with ^{14}C) were dissolved in the bathing fluid inside the alveolar sac. Double-tracer technique was utilized in every experiment. The pleural bathing solution was stirred by a fast stream of air bubbles saturated with water. The alveolar bathing solution was not directly stirred, but the lung sac was gently moved by the stream of air in the external fluid. Aliquots of pleural bathing fluid (250 μl) were sampled at hourly intervals for up to 5 h after adding the radiotracers to the alveolar fluid. The samples were placed in vials that contained 10-ml premixed scintillant solution (PCS, Amersham, Arlington Heights, IL) and counted in a liquid scintillation spectrometer (model LS250, Beckman, Irvine, CA).

The permeability-surface area products ($P \cdot S$) of water and solutes were estimated from the slopes of the graphs relating isotope concentration change in the pleural bathing solution to time. Assuming conservation of radioactive materials in the system and first-order kinetics for solute diffusion across the tissue, the following equation can be derived (1, 13)

$$\ln(1 - k \cdot \mathrm{C_c}/\mathrm{C_{h_0}})/t = -P \cdot S \cdot k/\mathrm{V_c} \qquad (1)$$

where $k = 1 + \mathrm{V_c}/\mathrm{V_h}$, $\mathrm{V_c}$ and $\mathrm{V_h}$ are the volumes of the cold (pleural) and hot (alveolar) bathing fluids, $\mathrm{C_c}$ is the concentration of the radiotracer in the pleural reservoir at time t, $\mathrm{C_{h_0}}$ is the concentration of radioactive solute in the alveolar sac at *time 0*, P is the permeability of the solute or water, and S is the total surface area for transfer of solute or water across the tissue.

To calculate absolute values of permeability, we estimated the surface area available for the diffusion of radiotracers across the alveolar epithelium at different lung volumes by assuming the lung sac preparations were spheres (see DISCUSSION below). The surface area for the 5-ml lungs was 14.14 cm^2, and that for the 50-ml lungs was 65.63 cm^2. Absolute permeability was calculated from the $P \cdot S$ product using these estimates of surface area. The surface area estimates were supported by light-microscopic observations of the tissue at different lung volumes that suggest that the lung pleats as it deflates [similar to the observations of Gil et al. (9) in mammalian lungs].

The presence of unstirred layers adjacent to the epithelial barrier necessitates correction of the permeability measurements to obtain true tissue permeability properties (12). We measured the thicknesses of the unstirred layers using the dilution potential technique of Smulders and Wright (26). The equation first proposed by Dainty (2) was then used to estimate the true permeabilities of the alveolar epithelium to water and solutes.

Estimation of pore radius. Assuming the presence of cylindrical water-filled pores in the alveolar epithelium, the equivalent homogeneous pore radius was estimated using the approaches developed by Renkin (21) and by Levitt (14). We note that permeability (P) of a nonelectrolyte through a barrier can be defined by the equation

$$\Phi = -P \cdot S \cdot \mathrm{dc} \qquad (2)$$

where Φ is the flux and dc is the concentration difference of the nonelectrolyte across the barrier. Furthermore, according to the first law of Fick, we can express the diffusional flux of a nonelectrolyte across a barrier as

$$\Phi = -D \cdot (A_s/\mathrm{d}x) \cdot \mathrm{dc} \qquad (3)$$

where D is the free diffusivity of the nonelectrolyte in

Downloaded from http://jap.physiology.org/ by 10.220.33.3 on September 15, 2016

water and A_s/dx is an equivalent surface area of water-filled channels through which the substance flows without interacting with the membrane divided by a homogeneous pore length or barrier thickness (3). Equating these two expressions for Φ, it can be seen that

$$A_s/dx = P \cdot S/D \tag{4}$$

Experimental values for A_s/dx can be obtained using *Eq. 4* from the measured $P \cdot S$ product for each substance divided by its known free diffusivity in water. It can be shown theoretically that, using certain assumptions,

$$A_s/dx = (A_p/dx) \cdot f(a/r) \tag{5}$$

where A_p is the total available pore area in the membrane, $f(a/r)$ is a factor that is related to the interaction between the solute and the pores (both resistances at the pore entrance and friction during pore transit), and a and r are the radii of the solute and the pores, respectively (14, 21). Renkin (21) used

$$f(x) = (1 - x)^2 \cdot (1 - 2.104x + 2.09x^3 - 0.95x^5) \tag{6}$$

while Levitt (14) later suggested an equation that leads to

$$f(x) = (1 - x)^2 \cdot (1 - 2.1054x + 2.0805x^3 - 1.7068x^5 + 0.72603x^6)/(1 - 0.75857x^5) \tag{7}$$

Now, taking the ratio of A_s/dx for each solute to that for water (i.e., using water as a reference substance), we obtain using *Eq. 5*

$$(A_s/dx)_{solute} = (A_s/dx)_{water} \cdot f(a/r)_{solute} / f(a/r)_{water} \tag{8}$$

thereby eliminating the unknown A_p. It should be noted that any of the substances studied could have arbitrarily been used as the reference solute. By use of this final theoretical relationship, a family of curves can be generated using different values for r and the molecular radii of water and the experimental solutes. By comparing the theoretical curves of A_s/dx vs. a with the experimental data, the best estimate of the equivalent homogeneous pore radius of the tissue can be obtained [using either the Levitt (14) or the Renkin (21) frictional factor expression].

RESULTS

Rates of radiotracer concentration changes in the pleural bath vs. time are shown in Fig. 2 (5-ml lung) and Fig. 3 (50-ml lung). The data shown are from different experiments for each solute. After about 1 h after the instillation of the alveolar fluid (containing radiotracer) and the suspension of the lung sac in the external Ringer solution, the relationship between radiotracer concentration (for each solute and water) and time becomes linear. The nonlinear portion during the 1st h is a frequently noted phenomenon (29) and is probably due to the adsorption of radiotracer onto the surfaces of the tissue and reservoirs.

From the slopes of these lines in Figs. 2 and 3, the $P \cdot S$ product of each solute and water was estimated using *Eq. 1*. The $P \cdot S$ products were divided by D as described above to obtain the relationship between A_s/dx and solute radius a to define the pore radius of the lungs (see *Eq. 4*). As shown in Figs. 4 and 5, the estimated homogeneous equivalent pore radii were 1.09 nm for 5-ml lungs and 0.89 nm for 50-ml lungs using *Eq. 6* (21). When *Eq. 7* (14) was used, the pore radii were 1.11 nm (5-ml lungs) and 0.93 nm (50-ml lungs). When arabinose was used as a reference solute (instead of water), there was no change

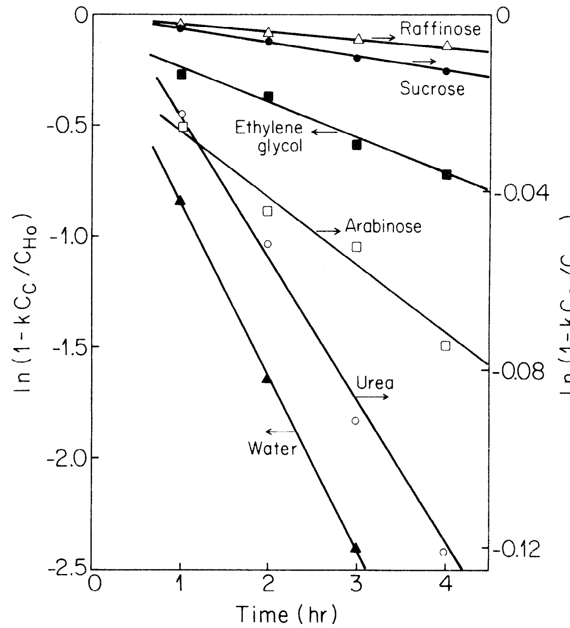

FIG. 2. Time courses of solute and water diffusion across sac-mounted bullfrog lung alveolar epithelium at 5 ml. Data shown are from different experiments for each solute. Slope of these curves of $\ln(1 - kC_c/C_{h_0})$ vs. time is $-kPS/V_c$ (where $k = 1 + V_c/V_h$, C's are concentrations of radiotracer, V's are volumes, PS is the permeability-surface area product, and subscripts c and h are cold and hot sides, respectively). *Arrows* in figure point to ordinate used for each solute (or water).

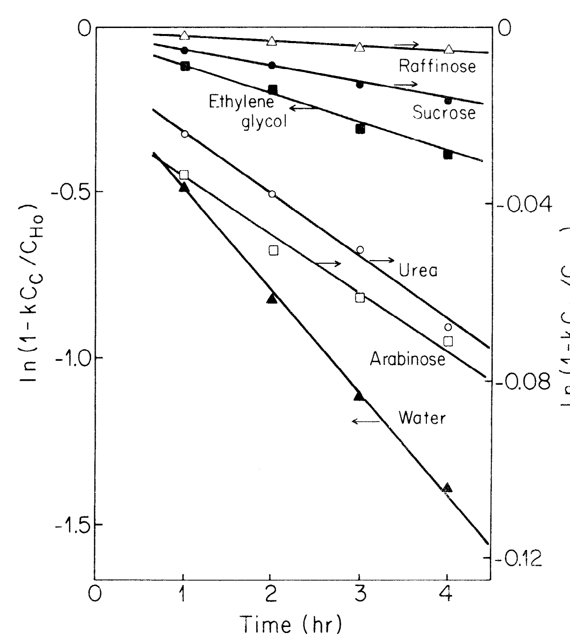

FIG. 3. Time courses of solute and water diffusion across the sac-mounted bullfrog lung alveolar epithelium at 50 ml. See Fig. 2 for further details.

Downloaded from http://jap.physiology.org/ by 10.220.33.3 on September 15, 2016

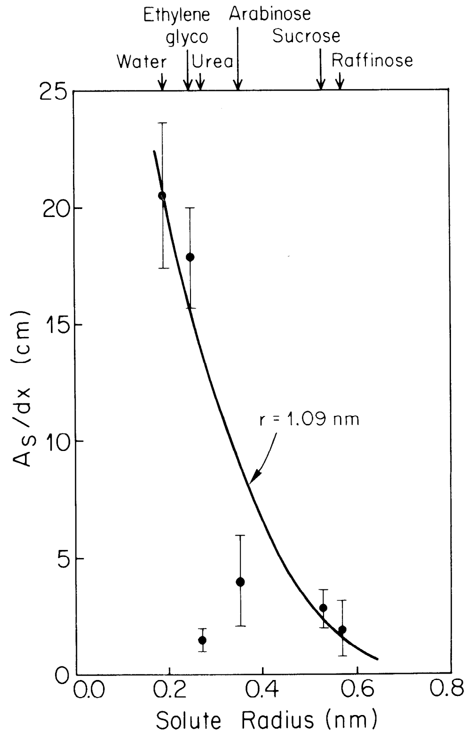

FIG. 4. A_s/dx plotted as a function of molecular radius for solute and water fluxes through sac-mounted bullfrog lung alveolar epithelium at 5 ml. *Solid line* represents theoretical relationship between A_s/dx and molecular radius in terms of Renkin pore model (21), assuming an equivalent pore radius of 1.09 nm. Each *point* represents mean ± SE for solute (or water). A_s/dx represents an equivalent surface area of water-filled channels through which substance flows without interaction with membrane, divided by a homogeneous pore length or uniform barrier thickness.

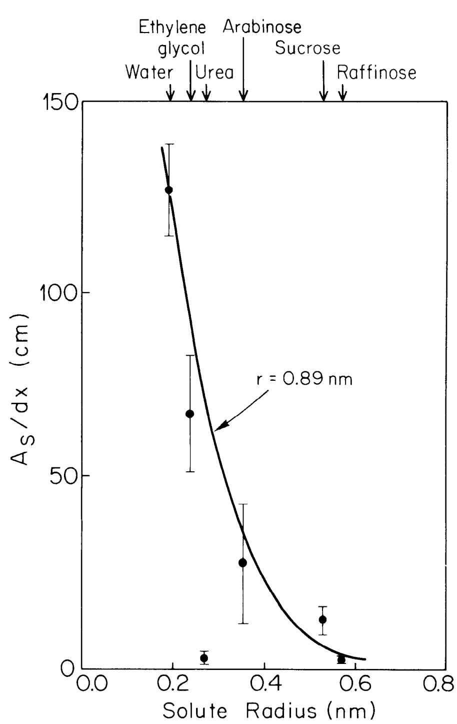

FIG. 5. A_s/dx plotted as a function of molecular radius for solute and water fluxes through sac-mounted bullfrog lung alveolar epithelium at 50 ml. Assumed pore radius of *solid line* is 0.89 nm. See Fig. 4 for further details.

in the calculated pore radii. Because of the apparently anomalous behavior of urea (see below) the theoretical pore radii were approximated without that solute, although inclusion of urea in the fit changed the values of the pore radii only slightly.

Once the lung has been subjected to overinflation to leakiness (above 80-ml lung volume) before reinflation to 50 ml, increased permeability to solutes and water results. Figure 6 shows the estimated pore radii for the control and the overinflated lungs. Compared with the control lungs inflated to 50 ml alone, those with a history of overinflation exhibited a larger pore radius, although free-diffusion characteristics were not attained. Overinflation caused the pore radius to increase from about 1 nm to about 3.4 nm (using *Eq. 6*; the increase was somewhat less using *Eq. 7*).

The unstirred layer thicknesses estimated in the 5-ml and 50-ml lungs were not significantly different, and averaged out to about 322 μm. The unstirred layer on the alveolar side of the tissue was 196 μm, and on the pleural side was 126 μm. The larger unstirred layer thickness on the alveolar side is likely due in part to the absence of vigorous mixing inside the lung sac.

As stated above, we estimated alveolar epithelial surface areas for the 5-ml and 50-ml lungs assuming they were spherical. This assumption of spherical diffusion surface for calculating S was supported by light-microscopic examination of the lungs fixed at different inflation volumes, which showed that the lung inflates by depleating (see DISCUSSION below). S turned out to be 14.14 cm^2 for 5-ml inflation and 65.63 cm^2 for 50-ml inflation. Our use of these estimates of S are necessary for the calculation of absolute P's and normalized R_t for comparison

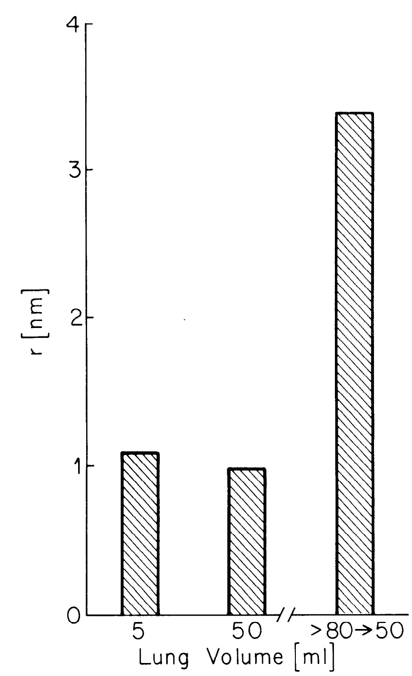

FIG. 6. Effect of bullfrog lung overinflation (>80 ml) on alveolar epithelial equivalent homogeneous pore radius. Pore radius of the 50-ml lungs was averaged (0.89 nm from those paired with 5-ml lungs and 1.04 nm from those paired with overinflated lungs). >80→50 denotes lungs inflated to 80 ml or more for 15 min, followed by reinflation to 50 ml.

Downloaded from http://jap.physiology.org/ by 10.220.33.3 on September 15, 2016

TABLE 1. *Alveolar epithelial transport properties at different physiological lung volumes*

	5-ml Lungs	50-ml Lungs
SPD, mV	13.9 ± 2.3 (9)	10.5 ± 3.3 (9)
R_t, kΩ·cm^2	3.92 ± 1.26 (4)	5.05 ± 0.79 (4)
P_{water}	327.1 ± 49.9 (12)	435.0 ± 41.5 (12)
$P_{ethylene\ glycol}$	143.9 ± 17.3 (3)	115.2 ± 25.9 (3)
P_{urea}	13.7 ± 4.1 (7)	6.2 ± 3.5 (7)
$P_{arabinose}$	22.1 ± 10.1 (3)	32.3 ± 18.0 (3)
$P_{sucrose}$	10.3 ± 3.1 (11)	10.2 ± 3.0 (11)
$P_{raffinose}$	5.9 ± 3.9 (3)	2.0 ± 0.3 (3)
r, nm	1.09	0.89

Values are means ± SE except for r. No. of observations given in parentheses. All P values expressed in cm/s × 10^{-7}, assuming surface area (S) = 14.14 cm^2 for 5-ml lungs and S = 65.63 cm^2 for 50-ml lungs. SPD, spontaneous potential difference; R_t, tissue resistance; P, permeability; r, radius.

TABLE 2. *Alveolar epithelial transport properties for control and overinflated lungs*

	Control Lungs	Overinflated Lungs
SPD, mV	8.3 ± 2.8 (4)	3.3 ± 1.6 (4)
R_t, kΩ·cm^2	2.98 ± 2.19 (4)	0.49 ± 0.25 (4)
P_{water}	658.6 ± 240.0 (3)	2294.3 ± 422.5 (3)
$P_{ethylene\ glycol}$	81.0 ± 13.1 (3)	308.9 ± 225.0 (3)
P_{urea}	31.5 ± 12.9 (3)	179.8 ± 72.9 (3)
$P_{arabinose}$	19.3 ± 14.3 (3)	225.6 ± 237.1 (3)
$P_{sucrose}$	11.5 ± 9.7 (3)	835.2 ± 596.1 (3)
$P_{raffinose}$	21.4 ± 10.5 (4)	180.7 ± 4.7 (4)
r, nm	0.97	3.38

Values are means ± SE except for r. No. of observations given in parentheses. Control and overinflated lungs studied at 50-ml volume. Overinflated lungs were previously inflated to >80-ml volume for 15 min before reinflation to 50-ml volume. All P values expressed in cm/s × 10^{-7}, assuming S = 65.63 cm^2. See Table 1 for abbreviations.

with previously reported data on lungs and other epithelial tissues (e.g., toad urinary bladder). The P's calculated from $P \cdot S$ and corrected for the unstirred layer effects are tabulated in Tables 1 and 2. There are no statistical differences between the P's for any solute or water (Table 1) for the 5-ml and 50-ml lung volumes ($P > 0.05$). On the otherhand, all P's (except ethylene glycol) are significantly different ($P < 0.05$) between the normal (50 ml) and overinflated lungs (Table 2). The correction of P for the unstirred layer effects was always ≤6.3%.

The SPD and R_t (Table 1) were 13.9 mV and 3.92 kΩ·cm^2 (5-ml lungs) and 10.5 mV and 5.05 kΩ·cm^2 (50-ml lungs), respectively. There are no significant differences ($P > 0.05$) between SPD or R_t at the two different lung inflation volumes. These data compare well to those reported previously for bullfrog alveolar epithelium (see DISCUSSION below). Both SPD and R_t of overinflated lungs (Table 2) were significantly less than those of control (50 ml) lungs.

DISCUSSION

Bullfrog lung alveolar epithelium showed no significant differences in bioelectric or passive water and solute permeability properties (or pore radii) at two different lung inflations within the physiological range. After overinflation followed by reinflation to physiological volume, SPD and R_t decreased and water and solute permeabilities (and pore radius) increased (Table 2). The SPD, R_t, and permeability properties obtained in this study using lung sacs are comparable with the results previously reported for the same tissue mounted as a flat sheet in the Ussing chamber (1). The sac preparation appears to be a viable model for the study of bullfrog lung alveolar epithelium.

The results obtained in this study are at variance with the conclusions based on data obtained in a recent sheep lung study. Egan et al. (5) suggested that the alveolar epithelial pore radius increases gradually with lung inflation volumes in the physiological range, whereas our data indicate no such change occurs. Although the use of equivalent homogeneous pore radius to characterize a tissue is greatly oversimplified and may be imprecise (see below), it can be of some usefulness for comparison purposes such as these.

As noted above, the mammalian lung preparation suffers from a number of practical problems. Of particular relevance to the effects of lung inflation on epithelial permeability is the fact that the alveolar fluid may have enormously thick unstirred layers adjacent to the pulmonary epithelia. The relative effects of these unstirred layers may vary with lung volume, leading to different degrees of underestimation of $P \cdot S$ at different lung inflations. Another major problem in interpreting the mammalian lung data is the presence of two parallel pathways for fluid and solute transport, namely, the airway vs. alveolar epithelium. The presence of the two epithelia, which have very dissimilar sieving properties [e.g., the hydraulic conductance of tracheal epithelium is about an order of magnitude higher than that of alveolar epithelium (1, 32)], may contribute to the differences in results obtained in the sheep lungs at different inflation volumes. This is especially true when it is recognized that the surface areas of contact between air-space fluid and alveolar epithelium on the one hand and between air-space fluid and small airway epithelium on the other hand are not well known and may change with lung inflation. A third important factor that may influence the results obtained in mammalian lungs is the use of different inflation pressures at different lung volumes. If the increment in interstitial and vascular hydrostatic pressure was not the same as that in the airway fluid, hydrostatic-pressure driving forces for fluid flow across the lung barriers would have been present that were different at different inflation volumes. This phenomenon could lead to altered solute fluxes due to solvent drag. The experiments reported in the present study were conducted in the absence of transepithelial pressure gradients. Finally, the recent observation by Gil et al. (9), in which it was shown that mammalian alveolar epithelium pleats and depleats with lung deflation and inflation, makes the suggestion that pore radius increases gradually with physiological lung inflation volumes more difficult to appreciate. With depleating, little tension should be present in the plane of the epithelium unless the alveolar epithelium is expanded to near or over total lung capacity. This observation lessens the likelihood that epithelial pore radius would increase gradually with physiological lung inflation.

Downloaded from http://jap.physiology.org/ by 10.220.33.3 on September 15, 2016

It must be noted that the differences between the previously reported data and our present data may be more apparent than real. First of all, the discrepancy may be due to the use of different animal species. Mammalian lungs (sheep and dog) may have permeability properties dissimilar to those of amphibian lungs (bullfrog). However, the general morphological and physiological similarity of the various alveolar epithelia (1, 31) tends to suggest that frog alveolar epithelium probably has transport properties that resemble those in mammalian lungs. Perhaps more important is that the data of Egan et al. (5), specifically their Figs. 5 and 6, can be interpreted somewhat differently and in a way that is more consistent with our own findings. Upon closer inspection, there appears to be little change in pore radius in sheep lungs until the lung inflation volume or pressure reaches a certain point (about 30 cmH_2O or 70% total lung capacity). After that, large increases in the pore radius are noted, reaching the equivalent of free diffusion at 40 cmH_2O or 100% total lung capacity. This interpretation suggests that mammalian and amphibian alveolar epithelium both remain tight until a certain inflation volume is reached, above which they both become leaky (see below). These findings are consistent with those obtained by Lewis et al. (16) in rabbit urinary bladder, in which it was determined that stretch of the tissue within the physiological range does not affect the resistance of the tight junction.

The more recent data on the effects of lung inflation on dog alveolar epithelial permeability (4) cannot be directly compared with our results, since we did not perform experiments on the same lung at different lung volumes. The dog lung data are still somewhat unexpected, since it is unlikely that damage to epithelial cell junctions occurs in the physiological range of lung inflation volumes. In our experiments, since no difference in pore radius of the paired lungs at 5-ml and 50-ml volumes was noted, we suspect that return of the 50-ml lung to 5-ml inflation volume would likewise not yield any difference in pore radius.

The overinflation of the bullfrog lung followed by reinflation to 50-ml lung volume led to an increase in the pore radius from about 1 nm to 3.4 nm. We did not observe increases in permeability properties to free diffusion, as reported by Egan et al. (5) for mammalian lungs. However, in both studies, it appears that the alveolar epithelial barrier is damaged by hyperinflation, probably at the tight junctions. Our speculation is that the lung alveolar epithelium depleats as it is inflated within the physiological range, after which tight junctions are irreversibly damaged by increasing tension within the plane of the epithelium.

To compare our transport properties, especially the permeability data, with data from other lung studies and from other tissues, reasonable estimates of the epithelial surface areas in the 5-ml and 50-ml lungs were needed. By approximating the lungs as spheres, we calculated surface areas of about 14 cm^2 (5-ml lungs) and about 66 cm^2 (50-ml lungs). The assumption of spherical available epithelial surface area for transport was based on our microscopic examination of fixed bullfrog lungs at different inflation volumes and on implications of the observations in mammalian lungs made by Gil et al. (9). The bullfrog lungs appear to pleat and depleat with deflation and inflation, similar to the phenomenon in mammalian lungs. This interpretation is supported by the observation that absolute tissue resistance was markedly different in the 5-ml and 50-ml lungs, but that normalized R_t was the same at both volumes (see below). The surface area available for solute and water flows thus varies with the degree of lung inflation. When nearing total lung capacity in our preparations, the entire alveolar wall may be available for transport. When pleated, however, surface area available for transport decreases because the portions of the alveolar epithelium which face each other cannot be utilized for effective ion, solute and/or water flow.

Using these estimates of surface area, we calculated normalized R_t and absolute values of permeability for water and solutes from $P \cdot S$. The results (see Table 1) were similar to those obtained when bullfrog lungs were studied as a flat sheet in the Ussing chamber. The pore radius from the present study is also in close agreement with that reported from the Ussing chamber studies (1). Furthermore, the data are comparable to those obtained from studies on another tight epithelium (toad urinary bladder), in which the epithelium is resistant to water and solute flows, with a pore radius of about 0.6–0.8 nm (11, 33). The lack of a good estimate of the surface area for water and solute flows in the mammalian lung preparation prevents direct comparison of our calculated absolute permeabilities with data from mammalian lung studies. It should be noted that all our measurements of solute and water diffusion in the present study were from alveolar to pleural fluid. This simplification is based on our observation that there is no directional dependence of diffusional fluxes across bullfrog alveolar epithelium (1).

As can be seen in Figs. 4 and 5 and Tables 1 and 2, urea permeability is very low compared with those for other solutes of comparable molecular size. The mechanism for this apparent anomalous behavior is unknown. The finding is very reproducible in our preparations, but has not been observed to our knowledge in other epithelia. One characteristic of urea that is of potential importance in this regard is its low solubility in oil relative to that of water and ethylene glycol. If direct permeation of membrane lipids plays a significant role in the transport of these solutes across alveolar epithelium, the lower permeability of urea would not be unexpected. Further experiments with lipophilic solutes will be necessary to resolve this point.

Several potential sources of error are present in our lung sac preparation. The bullfrog lung is hollow and thus provides a simple model for the study of the transport properties of alveolar epithelium. Although the lung is lined by a continuous layer of epithelial cells that have characteristics of both type I and type II pneumocytes of mammalian lungs, there are also a pleural mesothelium covering the outer lung surface and a connective tissue layer containing blood vessels, nerves, and smooth muscles between the epithelium and pleura. It is unlikely, however, that the tissue components other than the epithelium contribute significantly to the transport phenomena observed in this study. Kim et al. (13) showed that visceral pleural tissue is extremely leaky to water

Downloaded from http://jap.physiology.org/ by 10.220.33.3 on September 15, 2016

and solute flow. Hays and Franki (10) showed that toad urinary bladder stripped of its epithelium offers little resistance to water and solute flow compared with the intact tissue. Further evidence that alveolar epithelium is the barrier of importance in bullfrog lungs has been cited in detail previously (1).

We have found that the use of silicone high-vacuum grease at the tissue periphery minimizes edge damage effects (1, 13) in Ussing chamber studies similar to results reported by Lewis and Diamond (15). In this study, we used the same technique for mounting the lung as a sac by coating the surface of the bronchial plug with silicone grease. Although we did not check for edge effects, the values obtained for SPD, R_t, and P suggest that leakage through that pathway was negligible.

We have considerable misgivings about characterizing biological tissue with an equivalent homogeneous pore radius. We have used such a pore radius in the present study for comparison purposes, although it is likely that such comparisons are oversimplified. Close inspection of Figs. 4 and 5 suggests that there may be at least two populations of pore radii in the alveolar epithelium. Lack of sufficient data has prevented us from analyzing the tissue in this more complex manner at the present time.

In summary, the sac preparation of the bullfrog lung has served well as a model for studying alveolar epithelial transport properties at different lung volumes. The bioelectric and transport properties do not change with lung volume within the physiological range, whereas overinflation of the lung beyond its physiological limit causes an irreversible increase in pore radius along with decreases in SPD and R_t. These results strongly suggest that normal alveolar epithelium maintains its functional integrity within the physiological range of lung volume changes, but that damage may occur in the epithelium when it is stretched beyond its normal dimensions.

The authors thank Dr. E. M. Wright for several helpful discussions.

This work was supported in part by National Heart, Lung, and Blood Institute Research Grant HL-26223 and American Heart Association Grant 80-617. Dr. K.-J. Kim is a Postdoctoral Research Fellowship Awardee from American Heart Association GLAA Fellowship 654F2.

Address for reprint requests: E. D. Crandall, Dept. of Medicine, UCLA School of Medicine, Los Angeles, CA 90024.

Received 22 April 1981; accepted in final form 18 January 1982.

REFERENCES

1. Crandall, E. D., and K. J. Kim. Transport of water and solutes across bullfrog alveolar epithelium. *J. Appl. Physiol.: Respirat. Environ. Exercise Physiol.* 50: 1263–1271, 1981.
2. Dainty, J. Water relations of plant cells. *Adv. Bot. Res.* 1: 279–326, 1963.
3. Durbin, R. P., H. Frank, and A. K. Solomon. Water flow through frog gastric mucosa. *J. Gen. Physiol.* 39: 535–551, 1956.
4. Egan, E. A. Response of alveolar epithelial solute permeability to changes in lung inflation. *J. Appl. Physiol.: Respirat. Environ. Exercise Physiol.* 49: 1032–1036, 1980.
5. Egan, E. A., R. M. Nelson, and R. E. Olver. Lung inflation and alveolar permeability to non-electrolytes in the adult sheep in vivo. *J. Physiol. London* 260: 409–424, 1976.
6. Gatzy, J. T. Bioelectric properties of the isolated amphibian lung. *Am. J. Physiol.* 213: 425–431, 1967.
7. Gatzy, J. T. Ion transport across the excised bullfrog lung. *Am. J. Physiol.* 228: 1162–1171, 1975.
8. Gee, M. H., and N. C. Staub. Role of bulk fluid flow in protein permeability of the dog lung alveolar membrane. *J. Appl. Physiol.: Respirat. Environ. Exercise Physiol.* 42: 144–149, 1977.
9. Gil, J., H. Bachofen, P. Gehr, and E. R. Weibel. Alveolar volume-to-surface area relationship in air- and saline-filled lungs fixed by vascular perfusion. *J. Appl. Physiol.: Respirat. Environ. Exercise Physiol.* 47: 990–1001, 1979.
10. Hays, R. M., and N. Franki. The role of water diffusion in the action of vasopressin. *J. Membr. Biol.* 2: 263–276, 1970.
11. Hays, R. M., and A. Leaf. Studies on the movement of water through the isolated toad bladder and its modification by vasopressin. *J. Gen. Physiol.* 45: 905–919, 1962.
12. House, C. R. *Water Transport in Cells and Tissues.* London: Arnold, 1974, p. 104–114, 319–322, and 327–329.
13. Kim, K. J., A. M. Critz, and E. D. Crandall. Transport of water and solutes across sheep visceral pleura. *Am. Rev. Respir. Dis.* 120: 883–892, 1979.
14. Levitt, D. G. General continuum analysis of transport through pores. I. Proof of Onsager's reciprocity postulate for uniform pore. *Biophys. J.* 15: 533–551, 1975.
15. Lewis, S. A., and J. M. Diamond. Sodium transport by rabbit urinary bladder, a tight epithelium. *J. Membr. Biol.* 28: 1–40, 1976.
16. Lewis, S. A., D. C. Eaton, and J. M. Diamond. The mechanism of Na transport by rabbit urinary bladder. *J. Membr. Biol.* 28: 41–70, 1976.
17. Normand, I. C. S., R. E. Olver, E. O. R. Reynolds, and L. B. Strang. Permeability of lung capillaries and alveoli to nonelectrolytes in the foetal lamb. *J. Physiol. London* 219: 303–330, 1971.
18. Okada, Y., S. Yoshiko, S. Davido, J. Kim, and S. Ikeda. Comparative morphology of the lung with special reference to the alveolar epithelial walls. I. Lung of the amphibia. *Acta Tuberc. Jpn.* 11: 63–72, 1962.
19. Pietra, G. G., J. P. Szidon, E. J. Callahan, and A. P. Fishman. Permeability of the alveolo-capillary membrane to proteins. *J. Clin. Invest.* 50: 73, 1971.
20. Pietra, G. G., J. P. Szidon, M. N. Leventhal, and A. P. Fishman. Hemoglobin as a tracer in hemodynamic pulmonary edema. *Science* 166: 1643–1646, 1969.
21. Renkin, E. M. Filtration, diffusion and molecular sieving through porous cellulose membranes. *J. Gen. Physiol.* 38: 225–243, 1954.
22. Schneeberger, E. E. Ultrastructural basis for alveolar-capillary permeability to protein. In: *Lung Liquids, Ciba Foundation Symposium 38 (New Series).* Amsterdam, Netherlands: Excerpta Medica, 1976, p. 3–28.
23. Schneeberger, E. E. Structural basis for some permeability properties of the air-blood barrier. *Federation Proc.* 37: 2471–2478, 1978.
24. Schneeberger-Keeley, E. E., and M. J. Karnovsky. The ultrastructural basis of alveolar capillary membrane permeability to peroxidase used as a tracer. *J. Cell Biol.* 37: 781–793, 1968.
25. Schneeberger, E. E., and M. J. Karnovsky. The influence of intravascular fluid volume on the permeability of newborn and adult mouse lungs to ultrastuctural protein tracers. *J. Cell Biol.* 49: 319–334, 1971.
26. Smulders, A. P., and E. M. Wright. The magnitude of nonelectrolyte selectivity in the gallbladder epithelium. *J. Membr. Biol.* 5: 297–318, 1971.
27. Taylor, A. E., and K. A. Gaar. Estimation of equivalent pore radii of pulmonary capillary and alveolar membranes. *Am. J. Physiol.* 218: 1133–1140, 1970.
28. Theodore, J., E. D. Robin, R. Gaudio, and J. Acevedo. Transalveolar transport of large polar solutes (sucrose, insulin, and dextran). *Am. J. Physiol.* 229: 989–996, 1975.
29. Ussing, H. H., and B. Johansen. Anomalous transport of sucrose and urea in toad skin. *Nephron* 6: 317–328, 1969.
30. Wangensteen, O. D., L. E. Wittmers, Jr., and J. A. Johnson. Permeability of the mammalian blood gas barrier and its components. *Am. J. Physiol.* 216: 719–727, 1969.
31. Weibel, E. R. Morphometric estimation of pulmonary diffusion capacity. V. Comparative morphometry of alveolar lungs. *Respir. Physiol.* 14: 26–43, 1972.
32. Welsh, M. J., J. H. Widdicombe, and J. A. Nadel. Fluid transport across the canine tracheal epithelium. *J. Appl. Physiol.: Respirat. Environ. Exercise Physiol.* 49: 905–909, 1980.
33. Wright, E. M., and R. J. Pietras. Routes of nonelectrolyte permeation across epithelial membranes. *J. Membr. Biol.* 17: 293–312, 1974.

Downloaded from http://jap.physiology.org/ by 10.220.33.3 on September 15, 2016